Supporting Information

Orbital Modulation and Coupled Redox Cycling in Fe–Mn Dual-Atom Catalysts for Efficient Fenton-like Water Purification

Jianing Xu,[a] Yangyang Wang ,*[b] Qianqian Chen,[c] Heng Zheng*[c]

[a]*Department of Joint Osteopathy, Liuzhou Worker's Hospital, Liuzhou, 545005, China;*

[b]*College of Water Resources and Architectural Engineering, Tarim University, Alar, 843300, China;*

[c]*School of Medicine, Guangxi University of Science and Technology, Guangxi, 545006, China.*

*Corresponding authors.

Prof. & Dr: Yangyang Wang

College of Water Resources and Architectural Engineering, Tarim University

E-mail: wangyangyang0317@163.com (Y. Wang)

Prof. & Dr. Heng Zheng

School of Medicine, Guangxi University of Science and Technology

E-mail: zy101801@163.com (H. Zheng)

Texts caption

Text S1. Synthesis Procedure for the PAA Stock Solution.

Text S2. Analytical Methods for PAA Quantification.

Text S3. Electrochemical measurements.

Text S4. Detection method of SMX intermediate products.

Text S5. Theoretical calculation.

Text S6. Calculation of metal-normalized rate constant.

Text S7. Analysis of $^1O_2$ Trapping by DMA.

Text S8. Detection of $^1O_2$ Using the SOSG Probe.

Text S9. The recovery method of catalysts in the cycling experiments.

Text S1. Synthesis Procedure for the PAA Stock Solution.

The peracetic acid (PAA) stock solution was synthesized by reacting acetic acid (CH_3COOH) with hydrogen peroxide (H_2O_2), using sulfuric acid (H_2SO_4) as a catalyst. In a typical procedure, 60 mL of CH_3COOH was mixed with 40 mL of H_2O_2, followed by the dropwise addition of 1.67 mL of H_2SO_4 under constant stirring. The resulting mixture was aged and subsequently stored at 4 °C for future use.

Text S2. Analytical Methods for PAA Quantification.

The concentration of the PAA stock solution was determined by a two-step iodometric titration. In the first step, hydrogen peroxide (H_2O_2) present in the solution was quenched using potassium permanganate. This was followed by the titration of PAA with potassium iodide under acidic conditions. For monitoring residual PAA concentrations during reaction processes, the N,N'-diethyl-p-phenylenediamine (DPD) colorimetric method was applied. The assay was performed by introducing excess KI (20 g L^{-1}), DPD (1.1 g L^{-1}), and phosphate buffer (0.5 M, pH 6.5), with the resulting absorbance measured at 515 nm.

Text S3. Electrochemical measurements.

Electrochemical measurements were conducted with a CHI 660E electrochemical workstation in a standard three-electrode configuration. A Pt wire, a saturated calomel electrode (SCE), and a glassy carbon electrode served as the counter, reference, and working electrodes, respectively. A catalyst ink was prepared by dispersing 5 mg of the catalyst in a mixture of 980 μL ethanol and 20 μL of 5% Nafion solution under ultrasonication for 40 min to achieve a homogeneous slurry. Then, 20 μL of the resulting ink was drop-cast onto the conductive circular surface of the glassy carbon electrode. After drying completely, the working electrode was immersed in a 0.5 M Na_2SO_4 electrolyte for electrochemical testing.

Text S4. Detection method of SMX intermediate products.

The intermediate products of SMX in the Fe–Mn/N–C/PAA system were

characterized using ultra-high performance liquid chromatography coupled with mass spectrometry (UPLC–MS) under positive electrospray ionization (ESI+) mode. Before analysis, the mobile phase was subjected to sonication to eliminate dissolved gases. Chromatographic separation was achieved using a C18 HPLC capillary column (100 mm × 2.1 mm i.d., 5 μm; Thermo, USA). Mobile phase A consisted of a mixture of methanol/water mixture (v/v = 70/30), while mobile phase B contained an aqueous solution of 0.1% formic acid and 5×10^{-3} mol L^{-1} ammonium formate. The flow rate was set at 1 mL min^{-1}, with an injection volume of 20 μL. Detection was performed at an excitation wavelength of 264 nm.

Text S5. Theoretical calculation.

First-principles calculations based on spin-polarized density functional theory (DFT) were performed using the Vienna ab initio simulation package (VASP). The projector-augmented wave (PAW) method was employed together with the Perdew–Burke–Ernzerhof (PBE) generalized gradient approximation (GGA) for the exchange–correlation functional. A plane-wave cutoff energy of 400 eV was used for all computations. Structural relaxations were considered complete when the total energy change was less than 0.1 meV and the forces on all atoms were below 0.01 eV $Å^{-1}$. A 6 × 6 graphene supercell (14.807 × 14.807 Å) with a 12 Å vacuum layer was constructed as the base model. Single-atom Fe-N_4 and Mn-N_4 configurations, as well as three distinct types of Fe/Mn co-doped structures, were modeled on this substrate. All calculations utilized a 4 × 4 × 1 k-point mesh for Brillouin zone sampling.

The interaction between the catalyst and peracetic acid (PAA) was quantified by calculating the adsorption energy (E_{ads}). Specifically, the E_{ads} of PAA on the active site was computed using the equation:

$$E_{ads} = E_{(catalyst/PAA)} - E_{catalyst} - E_{PAA}$$

where $E_{(catalyst/PAA)}$ is the total energy of the optimized catalyst-PAA complex, $E_{catalyst}$ is the energy of the isolated catalyst model, and E_{PAA} is the energy of a single PAA molecule in the gas phase. A more negative Eads value corresponds to a more favorable and stronger adsorption configuration, which is crucial for the subsequent

activation step.

To gain deeper insight into the catalytic mechanism, we investigated the reaction pathway for PAA activation. The Gibbs free energy change (ΔG) for each elementary reaction step was determined by:

$$\Delta G = \Delta E + \Delta ZPE - T\Delta S$$

where ΔE is the reaction energy directly derived from DFT calculations, ΔZPE is the change in zero-point energy, T is the temperature (set to 298.15 K), and ΔS is the change in entropy. The Gibbs free energy profile was constructed to identify the rate-determining step and elucidate the catalytic efficiency of different active sites.

Text S6. Calculation of metal-normalized rate constant.

To compare the intrinsic catalytic activity of different catalysts, the observed pseudo-first-order rate constant was normalized by the total molar concentration of metal species in the reaction system:

$$k_{norm} = k_{obs}/C_{metal}$$

where k_{obs} is the apparent first-order rate constant (min^{-1}), and C_{metal} is the total molar concentration of metal species (mol L^{-1}) calculated from the catalyst dosage and the ICP-measured metal loading.

For the Fe–Mn/N–C catalyst, the total metal concentration was calculated as:

$$C_{metal} = C_{Fe} + C_{Mn}$$

with

$$C_{Fe} = C_{cat} \times w_{Fe}/M_{Fe},\ C_{Mn} = C_{cat} \times w_{Mn}/M_{Mn}$$

where C_{cat} is the catalyst dosage (g L^{-1}), w_{Fe} and w_{Mn} are the ICP-determined mass fractions of Fe and Mn, and M_{Fe} and M_{Mn} are the molar masses of Fe and Mn, respectively.

Text S7. Analysis of $^1O_2$ Trapping by DMA.

9,10-Dimethylanthracene (DMA) was employed as a selective molecular probe for $^1O_2$, undergoing a specific reaction to form its endoperoxide derivative (DMA–O_2).

The formation of DMA–O_2 was analyzed using mass spectrometry with atmospheric pressure chemical ionization in positive ion mode (APCI+), acquiring signals across a mass range of 100–450 m/z. Retention times for DMA and DMA–O_2 were determined from their respective MS signals. The conversion extent from DMA to DMA–O_2 was quantified based on absorbance measurements at 258 nm, using the molar absorption coefficients εDMA, 258 nm and εDMA–O_2, 258 nm. Experimentally, 1 mL of a DMA solution (3.2 μmol L^{-1}) was added to 1.0 mL of the reaction mixture. Fluorescence detection was carried out with excitation at 380 nm and emission monitored at 425 nm, providing an additional spectroscopic signal for monitoring the reaction.

Text S8. Detection of $^1O_2$ Using the SOSG Probe.

$^1O_2$ generation was monitored using the Singlet Oxygen Sensor Green (SOSG) fluorescent probe. Prior to each experiment, a 500 μM SOSG stock solution was prepared in deoxygenated methanol. For the reaction, 1 mg of catalyst and 200 μL of the SOSG stock solution were added to 10 mL of ultrapure water. The reaction was initiated by introducing 20 μL of 100 mM PAA.

At designated time intervals, 500 μL aliquots were collected, diluted to 4 mL with ultrapure water, and immediately filtered through a 0.22 μm PTFE syringe filter. Fluorescence measurements were conducted on a HITACHI F-4600 spectrofluorometer with an excitation wavelength of 488 nm, and the emission spectrum was recorded from 500 to 590 nm.

Text S9. The recovery method of catalysts in the cycling experiments.

After the 20-min reaction, the catalysts were separated from the solution by suction filtration. They were subsequently washed with deionized water several times and transferred into a new solution via brief sonication (2–3 s) to detach them from the filter paper.

Figures caption

Fig. S1 Atomic structure model of the Fe–Mn/N–C dual-atom catalyst.

Fig. S2 a-c Bader charge analysis of Fe/N–C, Mn/N–C, and Fe–Mn/N–C.

Fig. S3 PAA adsorption energies on Fe/N–C, Mn/N–C, and Fe–Mn/N–C.

Fig. S4 The O–O bond length of adsorbed PAA on Fe/N–C, Mn/N–C, and Fe–Mn/N–C.

Fig. S5 PDOS of Mn/N–C and Fe–Mn/N–C.

Fig. S6 a-f SEM and TEM images of Fe/N–C, Mn/N–C and Fe–Mn/N–C.

Fig. S7 a-c Full survey, High-resolution C 1s, and O 1s XPS spectra of Fe/N–C, Mn/N–C, and Fe–Mn/N–C.

Fig. S8 a-b Influence of Fe–Mn/N–C dosage and PAA concentration.

Fig. S9 SMX removal efficiency in only-PAA system.

Fig. S10 Kinetic curves in different reaction systems.

Fig. S11 TOC removal of different reaction systems.

Fig. S12 SMX degradation efficiency in Fe–Mn/N–C/PAA/D_2O system.

Fig. S13 Metal leaching during cyclic operation of the Fe–Mn/N–C/PAA system.

Fig. S14 Metal leaching under different pH conditions in the Fe–Mn/N–C/PAA system.

Fig. S15 Effect of humic acid on SMX degradation in the Fe–Mn/N–C/PAA system.

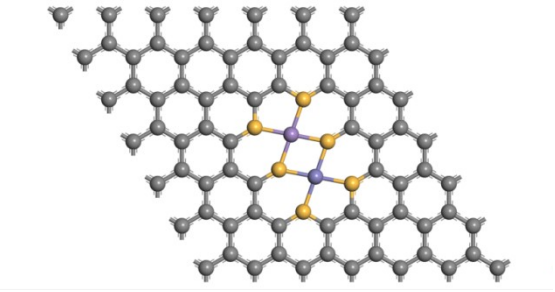

Fig. S1 Atomic structure model of the Fe–Mn/N–C dual-atom catalyst.

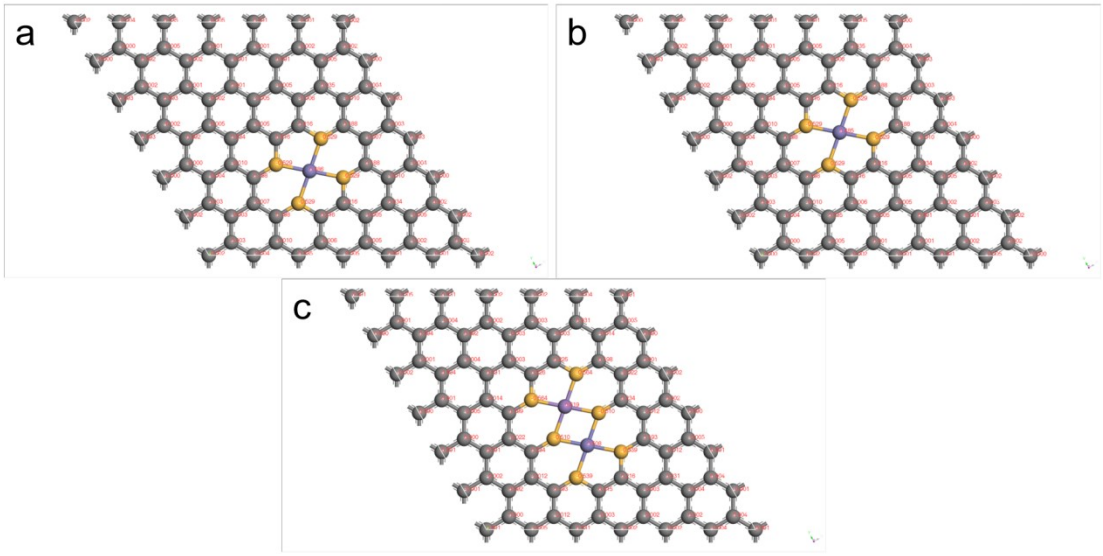

Fig. S2 a-c Bader charge analysis of Fe/N–C, Mn/N–C, and Fe–Mn/N–C.

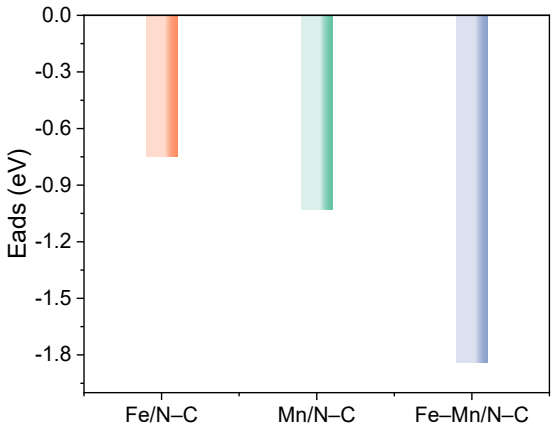

Fig. S3 PAA adsorption energies on Fe/N–C, Mn/N–C, and Fe–Mn/N–C.

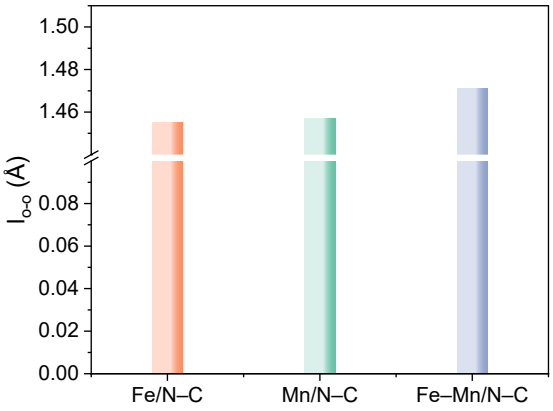

180

181 **Fig. S4** The O–O bond length of adsorbed PAA on Fe/N–C, Mn/N–C, and Fe–Mn/N–

182 C.

183

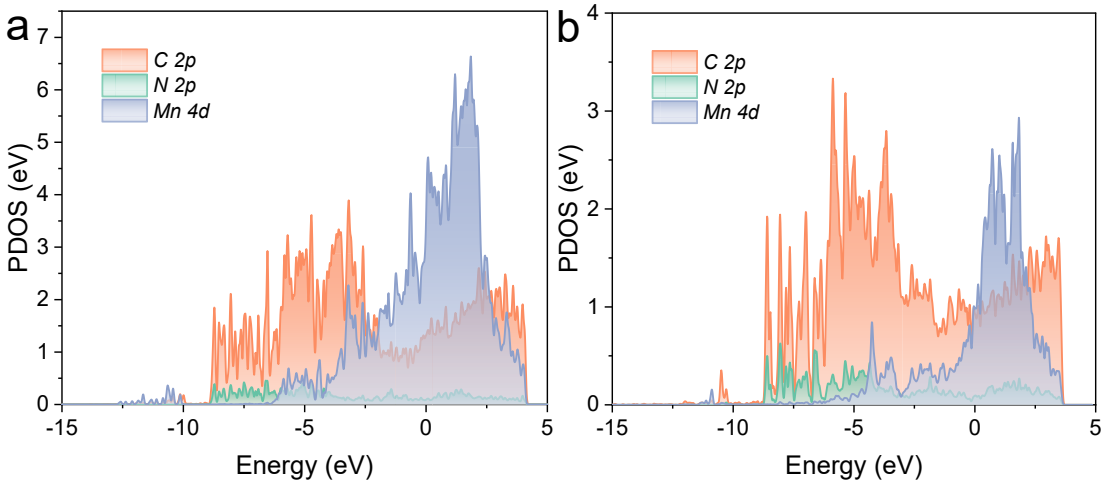

184

185 **Fig. S5** PDOS of Mn/N–C and Fe–Mn/N–C.

186

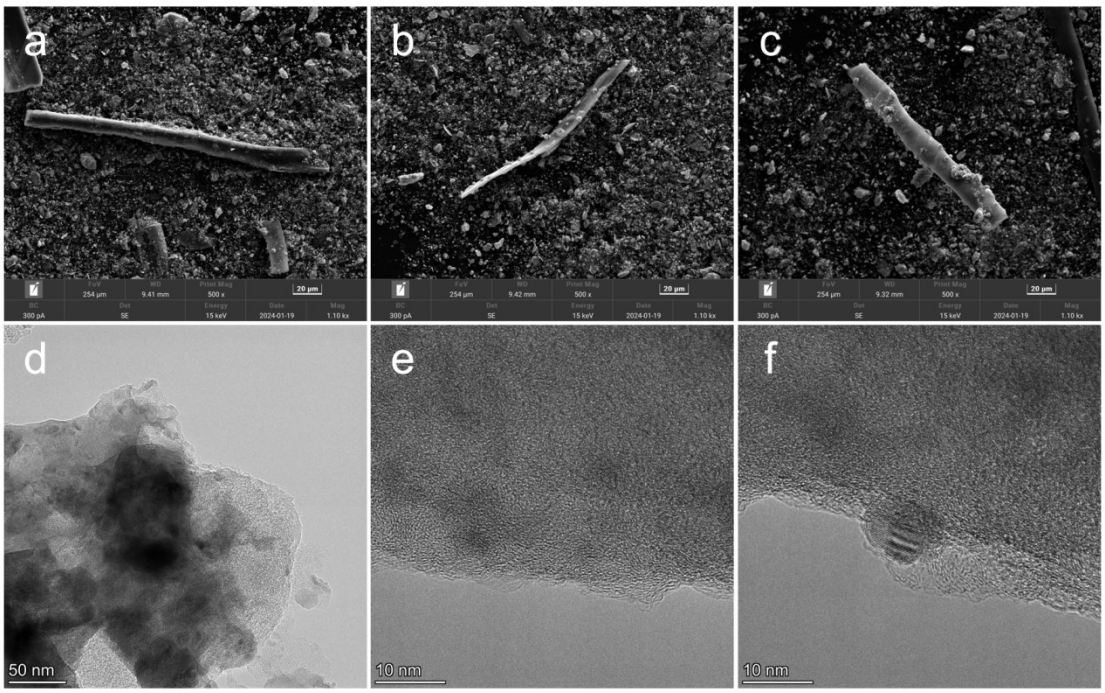

Fig. S6 a-f SEM and TEM images of Fe/N–C, Mn/N–C and Fe–Mn/N–C.

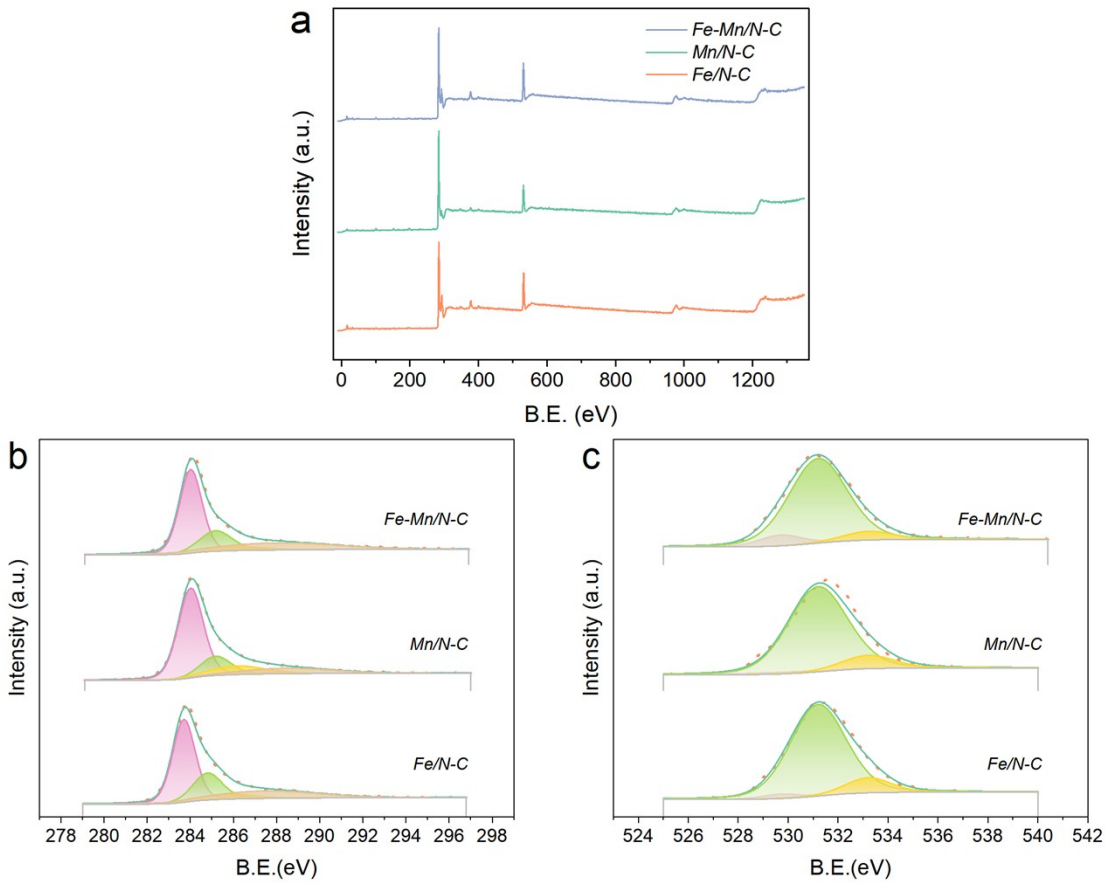

Fig. S7 a-c Full survey, High-resolution C 1s, and O 1s XPS spectra of Fe/N–C, Mn/N–C, and Fe–Mn/N–C.

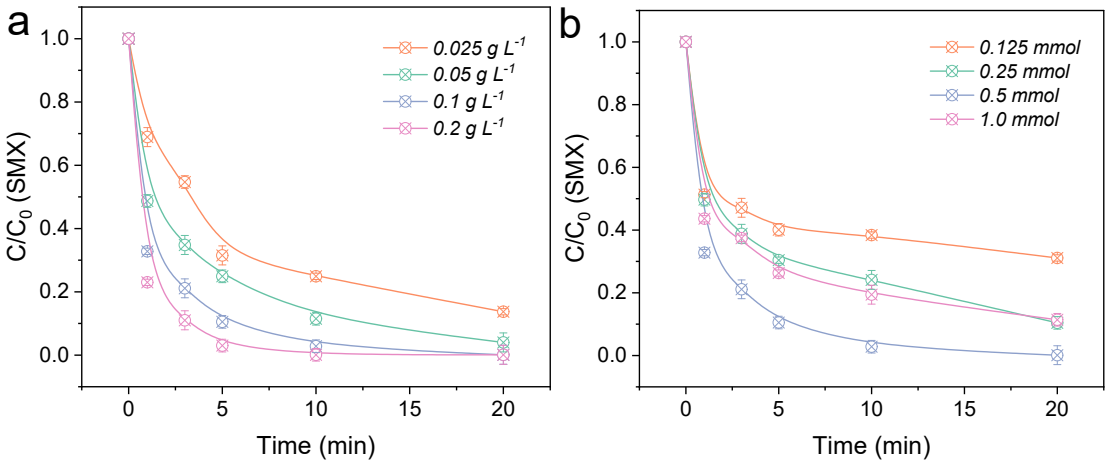

Fig. S8 a-b Influence of Fe–Mn/N–C dosage and PAA concentration.

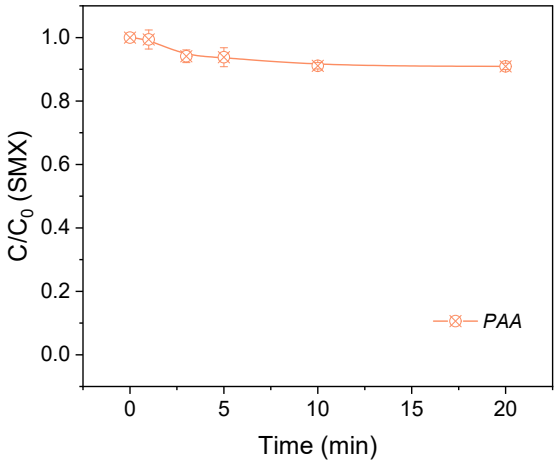

Fig. S9 SMX removal efficiency in only-PAA system.

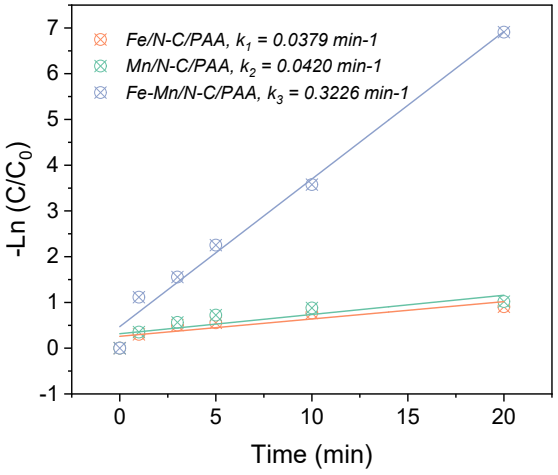

Fig. S10 Kinetic curves in different reaction systems.

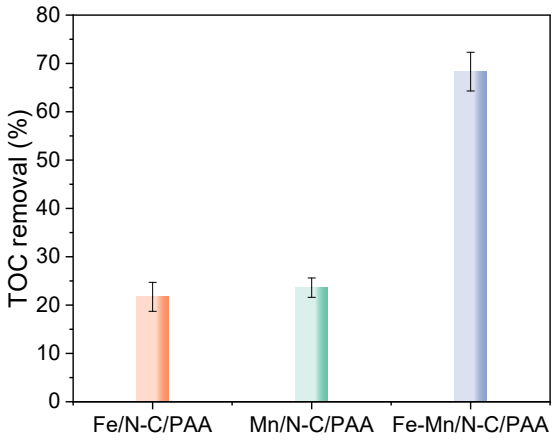

Fig. S11 TOC removal of different reaction systems.

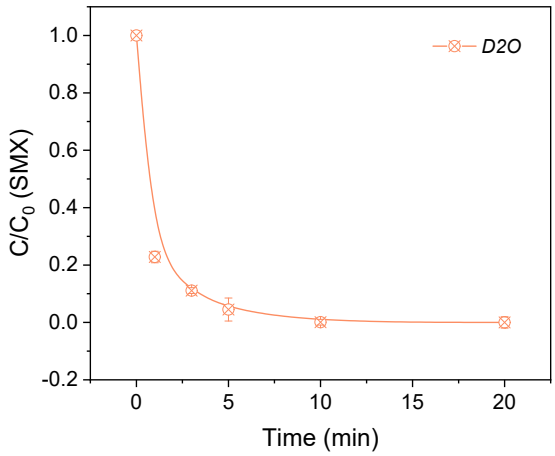

Fig. S12 SMX degradation efficiency in Fe–Mn/N–C/PAA/D_2O system.

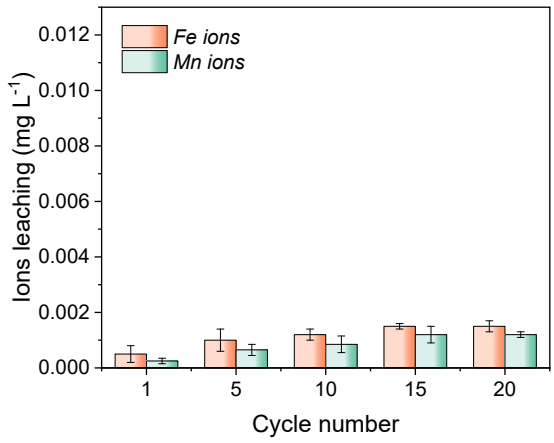

Fig. S13 Metal leaching during cyclic operation of the Fe–Mn/N–C/PAA system.

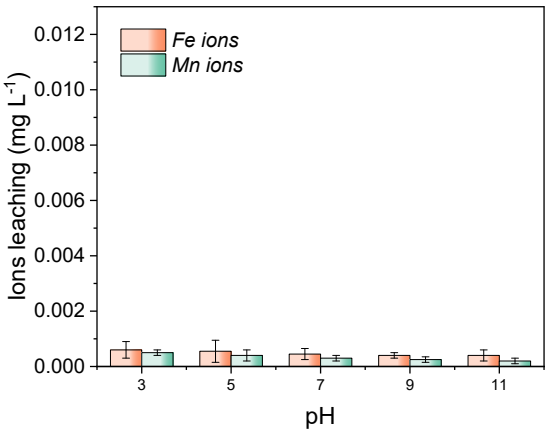

Fig. S14 Metal leaching under different pH conditions in the Fe–Mn/N–C/PAA system.

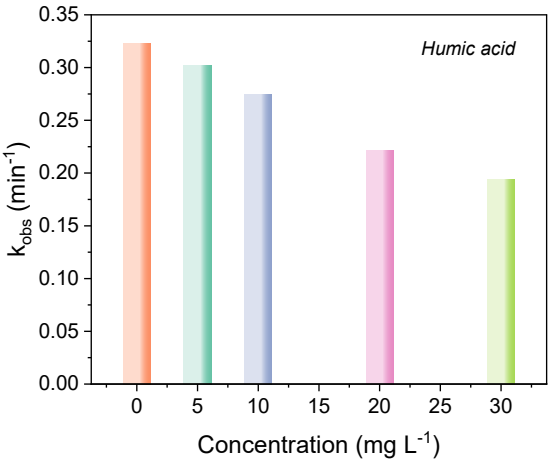

Fig. S15 Effect of humic acid on SMX degradation in the Fe–Mn/N–C/PAA system.

Tables caption

Table S1. Porous properties of Fe/N–C, Mn/N–C, and Fe–Mn/N–C.

Table S2. EXAFS fitting parameters of Fe and Mn K-edge for Fe–Mn/N–C.

Table S3. Metal loading, kinetic constants, and normalized rate constants of different catalysts.

Table S4. Empirical formulae and m/z values for protonated molecular ions and characteristic fragments of the identified products.

Table S5. Physical and chemical properties of different pollutants.

Table S6. Calculated parameters of different organics.

Table S1. Porous properties of Fe/N–C, Mn/N–C, and Fe–Mn/N–C.

Catalyst	Specific surface area[a] /m^2 g^{-1}	Pore volume[b] /cm^3 g^{-1}	Pore diameter[c] /nm
Fe/N–C	13.6	0.24	4.3
Mn/N–C	15.8	0.27	5.1
Fe–Mn/N–C	20.7	0.17	3.7

[a]Specific surface area calculated from the nitrogen adsorption isotherm using the BET method. [b]Pore volume obtained from BJH desorption cumulative volume of pores. [c]Data obtained from BJH desorption average pore diameter.

Table S2. EXAFS fitting parameters of Fe and Mn K-edge for Fe–Mn/N–C.

Sample	Path	N[a]	R/Å[b]	σ^2/Å^{2c}	R-factor
Fe in Fe–Mn/N–C	Fe-Mn	0.9 ± 0.2	2.43 ± 0.03	0.007	0.006
Mn in Fe–Mn/N–C	Mn-Fe	1.1 ± 0.2	2.43 ± 0.03	0.006	0.008

[a]N is the coordination number. [b]R is the distance betweenabsorber and backscatter atoms, [c]σ^2 is the Debye-Waller factor, R-factor is residual factor.

Table S3. Metal loading, kinetic constants, and normalized rate constants of different catalysts.

Catalyst	Metal loading (wt%)	C_{metal} (10^{-5} mol L^{-1})	k_{obs} (min^{-1})	k_{norm} (L mol^{-1} min^{-1})
Fe/N-C	2.7	4.82	0.0379	786
Mn/N-C	2.5	4.55	0.0420	923
Fe-Mn/N-C	Fe: 2.7, Mn: 2.5	8.09	0.3226	3988

Table S4. Empirical formulae and m/z values for protonated molecular ions and characteristic fragments of the identified products.

Formula	Intermediate product	ESI m/z	Structure
$C_{10}H_{11}N_3O_3S$	Sulfamethoxazole	254	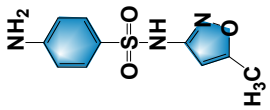
$C_{10}H_9N_3O_5S$	P1	283	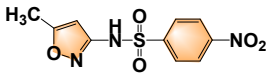
$C_{10}H_9N_3O_6S$	P2	299	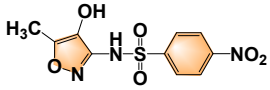
$C_6H_7NO_3S$	P3	173	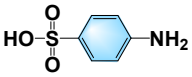
$C_4H_5N_2O$	P4	98	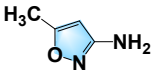
$C_4H_4N_2O_3$	P5	128	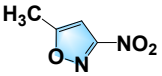
$C_7H_6O_2$	P6	122	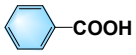
C_6H_7NO	P7	109	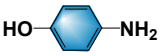
$C_4H_6N_2O_3S$	P8	162	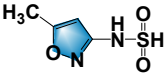
$C_{10}H_9N_3O_5S$	P9	283	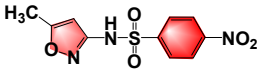
$C_{10}H_9N_3O_6S$	P10	299	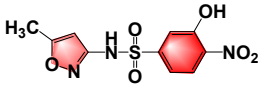
$C_{10}H_{10}N_2O_3S$	P11	238	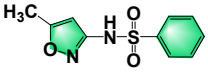
$C_{10}H_{11}N_3O_4S$	P12	269	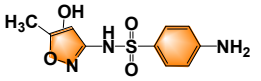
$C_{10}H_{13}N_3O_5S$	P13	287	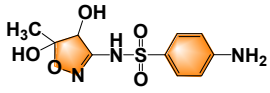

$C_{11}H_8N_3O_{11}S$	P14	130	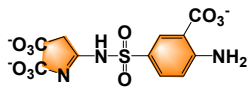

243

244

245 **Table S5.** Physical and chemical properties of different pollutants.

Chemical Name	Chemical structure	Molecular formula	Molecular weight (g mol^{-1})
Sulfadiazine	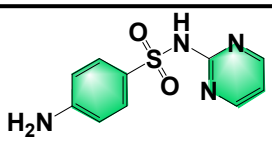	$C_{10}H_{10}N_4O_2S$	250.28
Sulfamethoxazole	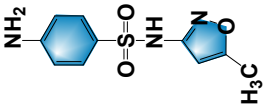	$C_{10}H_{11}N_3O_3S$	253.28
Sulfamerazine	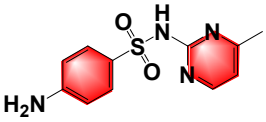	$C_{11}H_{12}N_4O_2S$	264.30
Sulfathiazole	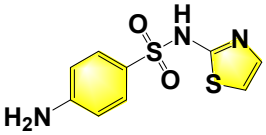	$C_9H_9N_3O_2S_2$	255.01
Sulfamethazine	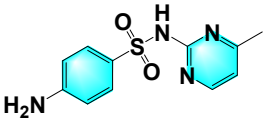	$C_{12}H_{14}N_4O_2S$	278.33
Sulfanilylacetamide	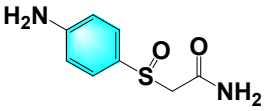	$C_8H_{10}N_2SO_3$	214.24
4-Chlorophenol	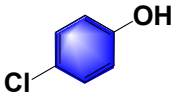	C_6H_5ClO	128.56
Bisphenol A	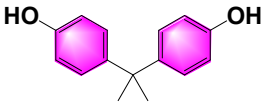	$C_{15}H_{16}O_2$	228.29

246

247

248 **Table S6.** Calculated parameters of different organics.

Chemical Name	HOMO eV	LUMO eV	ΔE ($E_{HOMO} - E_{LUMO}$)
Sulfadiazine SDZ	-6.25	-1.61	-4.64
Sulfamethoxazole SMX	-6.27	-1.19	-5.08
Sulfamerazine SD1	-6.25	-1.51	-4.74
Sulfathiazole STZ	-6.26	-1.27	-4.56
Sulfamethazine SD2	-6.24	-1.40	-4.84
Sulfanilylacetamide SMD	-6.27	-1.74	-4.53
4-Chlorophenol 4-CP	-6.33	-1.07	-5.26
Bisphenol A BPA	-6.03	-0.60	-5.43

249

250